InGaAs/InP MONOLITHIC INTERCONNECTED MODULES (MIM) FOR THERMOPHOTOVOLTAIC APPLICATIONS

David M. Wilt
NASA Lewis Research Center
Cleveland, Ohio 44135

Navid S. Fatemi, Phillip P. Jenkins, Victor G. Weizer, and Richard W. Hoffman, Jr.
Essential Research, Inc.
Cleveland, Ohio 44122

David A. Scheiman
NYMA, Inc.
Brook Park, Ohio 44142

Christopher S. Murray and David R. Riley
Westinghouse Electric Corporation
West Mifflin, PA 15122

Abstract

There has been a traditional trade-off in thermophotovoltaic (TPV) energy conversion development between system efficiency and power density. This trade-off originates from the use of front surface spectral controls such as selective emitters and various types of filters. A monolithic interconnected module (MIM) structure has been developed which allows for both high power densities and high system efficiencies. The MIM device consists of many individual indium gallium arsenide (InGaAs) devices series-connected on a single semi-insulating indium phosphide (InP) substrate. The MIMs are exposed to the entire emitter output, thereby maximizing output power density. An infrared (IR) reflector placed on the rear surface of the substrate returns the unused portion of the emitter output spectrum back to the emitter for recycling, thereby providing for high system efficiencies.

Initial MIM development has focused on a 1 cm^2 device consisting of eight series interconnected cells. MIM devices, produced from 0.74 eV InGaAs, have demonstrated V_{oc} = 3.2 volts, J_{sc} = 70 mA/cm^2 and a fill factor of 66% under flashlamp testing. Infrared (IR) reflectance measurements (>2 μm) of these devices indicate a reflectivity of >82%. MIM devices produced from 0.55 eV InGaAs have also been demonstrated. In addition, conventional p/n InGaAs devices with record efficiencies (11.7% AM0) have been demonstrated.

Introduction

In thermophotovoltaic energy conversion, an emitter is heated to incandescence and a photovoltaic device is placed in view of the emitter to convert the radiant energy into electrical energy. Research in TPV has been renewed recently, due to the development of new emitter, filter and photovoltaic cell technology. Most current efforts in TPV research have concentrated on using front surface spectral control elements such as selective emitters[1] or graybody emitters combined with plasma, dielectric or dipole filters[2, 3] in order to improve system efficiency to the 20–40% range predicted by theory[4].

The front-surface spectral control approach tends to produce systems with low power density (W/cm^2). Selective emitters, for example, have demonstrated in-band emittances which range from 0.7 to 0.8,[5] with efficiencies of ~40% (i.e. 40% of the emitted energy is convertible by the photovoltaic device). In order to

recuperate the non-convertible energy, filters are used to reflect the long-wavelength photons back to the selective emitter. Unfortunately, there are no filters available which provide both 100% transmission in the usable wavelength region and 100% reflection everywhere else. Thus, a selective emitter emitance of 0.8, coupled with a typical filter transmission of 80% leads to a reduction in the power density of 36%. This is an expensive loss, particularly given the cost of TPV cells. Grey body emitter based systems have similar power density problems.

A different approach involves the use of rear-surface spectral controls. Using this technique, the entire radiant output from the emitter is incident upon the photovoltaic (PV) device, thereby providing high output power densities. Photons which the PV device is unable to convert pass through the cell structure, reflect off of a rear reflector and are returned to the emitter for recycling. Researchers have developed TPV cells which utilize low-doped substrates and reflective rear contacts to provide photon recycling[6, 7]. Other researchers have developed series-interconnected, monolithic cells for laser, fiber-optic and TPV applications[8, 9]. We are developing a cell which combines the advantages of both of these approaches.

The Monolithic Interconnected Module or MIM consists of series-connected indium gallium arsenide (InGaAs) devices on a common, semi-insulating indium phosphide (InP) substrate (Fig. 1). An infrared reflector is deposited on the rear surface of the InP substrate to reflect photons back toward the front surface of the cell. This provides a second pass opportunity for photons capable of being converted by the cell. In addition, long wavelength photons are returned to the emitter for "recycling", improving the system efficiency.

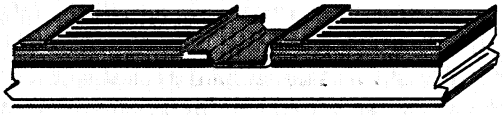

a

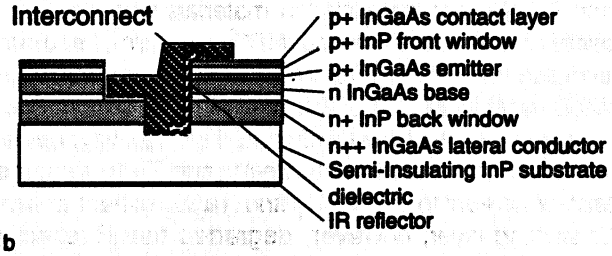

b

Figure 1.—a) 3-dimensional view of two cells of a MIM. b) a cross-sectional view of a MIM showing the individual layers and interconnect scheme.

The MIM design offers several advantages compared to conventional TPV cell designs. First, small series-connected cells provide high voltages and low currents, thereby reducing I^2R losses. In addition, the small size of the cells allow an array to be comprised of series/parallel strings rather than a single series-connected string of larger cells. This should improve the reliability of the TPV module since the failure of a single cell would not debilitate the entire array. Second, the MIM design maximizes output power density since losses associated with front-surface spectral controls are eliminated.

Third, the rear surface of the device is not electrically active, therefore the cell may be directly bonded to the substrate/heat sink without concern for electrical isolation. This greatly simplifies the array design and improves the thermal control of the cells. Fourth, the array may easily be designed with differing cell sizes to reduce view factor losses and losses associated with non-uniform emitter temperatures. Last, photons which are weakly absorbed have the possibility of multiple passes through the cell structure. This feature is particularly important for lattice-mismatched devices, where poor minority carrier diffusion length can be partially offset by making the cell thin, forcing the carrier generation to occur closer to the p/n junction.

Materials Development

The MIM structures were deposited in a horizontal, low-pressure organo-metallic vapor phase epitaxy (OMVPE) reactor described elsewhere[10]. The precursor materials were trimethyl indium (TMIn), trimethyl gallium (TMGa), arsine, phosphine, diethyl zinc (DEZn) and silane for p and n doping respectively. Several test growths were conducted to determine the compositional, thickness and doping uniformity of InGaAs across the 2-in. diameter substrate. Secondary electron microscopy analysis indicates the thickness variation was ±3% in the axial direction and ±9% in the perpendicular direction (exclusive of a 5-mm wide region at the perimeter of the substrate). These results were consistent from run to run. Double crystal x-ray rocking curve measurements indicated a variation in InGaAs composition of ±0.7% (relative) in the axial direction and ±0.4% (relative) in the perpendicular direction. This compositional uniformity was reproducible from run to run, although we did observe a variation in the absolute composition of ±0.5% In. This was attributed to a variation in the transport efficiency of the TMIn source.

Hall measurements were conducted for both n-type (Si doped) and p-type (Zn doped) InGaAs to map the doping distribution over the 2-in. diameter substrates. The results indicate a variation of ±14% in the axial direction and ±42% in the perpendicular direction for the n-type material and ±2% in the axial direction and ±4% in the perpendicular direction for the p-type material. The p-type result is consistent with the compositional and thickness uniformity observed for this sample. The variation observed for the n-type material in the perpendicular direction is believed to be due to enhanced SiH_4 cracking caused by the close proximity of the hot chamber walls. We are examining the use of alternative dopants or modified reactor geometry to reduce this variation.

The MIM device requires dielectric isolation for the interconnect. Three different dielectrics were tested for their suitability. The three materials were e-beam evaporated Ta_2O_5, spin on glass (SOG) and plasma-enhanced chemical vapor deposited (PECVD) Si_3N_4. A test structure was developed to characterize the deposited material for dielectric constant, resistivity and breakdown strength, as well as to test for the presence of pin hole defects. Both the Ta_2O_5 and SOG contained many pinholes and shunting paths. A suitable layer of Si_3N_4 was developed which demonstrated a resistivity of $>10^{10}$ ohm-cm.

Several different contact and IR reflector metallization materials were tested. The important requirements for these materials were: 1) low specific contact resistance (10^{-6} ohm-cm^2) for both n and p-type InGaAs, 2) good adhesion between the metallization and the InP, InGaAs and the dielectric, and 3) good IR reflection (>95%) for the IR reflector material. The initial tests were conducted with the Au-Ge-Au contacts used in our planar cell development[11]. This material provided excellent contact resistivity and IR reflectivity, but had poor adhesion to the dielectric. We also tested Ag-Au, Cr-Au and Ti-Au and found that the Cr-Au and Ti-Au demonstrated acceptable resistivity (mid 10^{-6} ohm-cm^2) as well as excellent adhesion to the Si_3N_4 and Ta_2O_5 dielectric films and is being used for the MIM contacts. The addition of the Cr sticking layer, however, degraded the IR reflectivity. The devices reported here utilized an Au IR back surface reflector (BSR).

Device Design

A p/n cell configuration (Fig. 1) was chosen for several reasons. First, the free carrier absorption for n-type InGaAs is significantly lower than for p-type, as will be addressed in the following section. Thus, the p/n configuration minimizes the areal density of holes, making it optimum in terms of optical recuperation. Second, the MIM design requires a thick rear conductor layer to conduct current the length of the device (laterally), to reach the back contact/interconnect. The p/n configuration takes advantage of the 25× higher mobility for n-type InGaAs in this conductor layer, reducing the resistive losses.

Finally, an increase in the optical bandgap of the n^{++} conductor layer material (see below) permits the use of a thin base region. Bandedge photons which are not absorbed in the base region are able to pass through the n^{++} layer without being absorbed. These photons reflect off the rear reflector and have a second chance of being absorbed in the base region.

Initial device configurations for both 0.74 and 0.55 eV InGaAs MIM's illuminated by a 1200 °K blackbody were developed (Fig. 2). The thickness' and doping levels of the lateral conduction layers and emitter layers were chosen to limit the resistive losses to 1% for each layer. The base thickness (2 microns) was intentionally produced for incomplete absorption in a single pass in order to take advantage of the BSR.

The optical efficiency of the 0.74 eV MIM device (long wavelength reflectivity) was modeled by determining the free carrier absorption (FCA) for both n- and p-type InGaAs as a function of dopant type, level, thickness and wavelength. Calibration samples with doping levels ranging from 5×10^{18} to 3×10^{19} cm^{-3} were fabricated on semi-insulating InP substrates. Absorption measurements were conducted using a spectrophotometer for the near IR (1–3 μm) and an FTIR for the mid IR (3–10 μm).

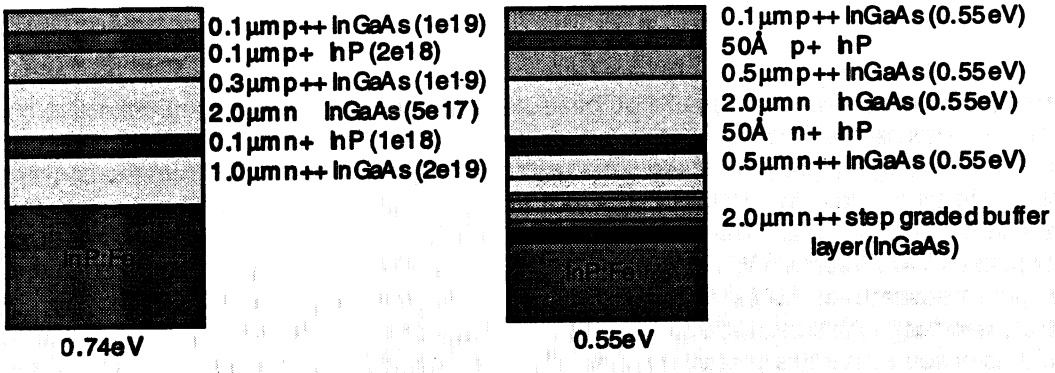

Figure 2.—0.74 and 0.55 eV device structures for operation with a 1200 K blackbody.

The spectrophotometer absorption data (Fig.3) shows several interesting features. First, the absorption for p-type material is significantly higher than for n-type material. Second, the n-type material has an apparent bandgap which is significantly higher (0.3 eV) than the equivalent composition p-type material. This shift in absorption is due to a Burstein-Moss shift.

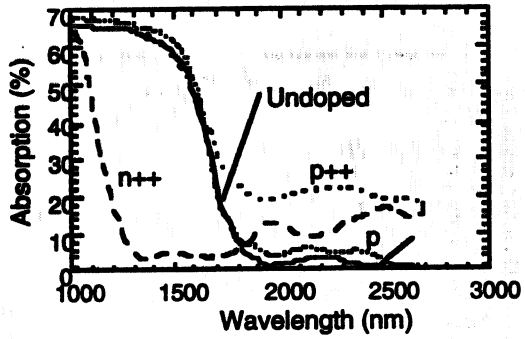

Figure 3.—Absorption data for $In_{0.55}Ga_{0.45}As$ with various doping types and densities.

Device Performance

Conventional planar p/n InGaAs devices were produced using the active cell layers shown in Figure 2a (note: the emitter doping was reduced to 1×10^{18} cm^{-3} for these devices) in order to verify the basic material quality. The I-V curve shown in Figure 4 demonstrates the quality of the baseline devices. The efficiency (11.7% AM0) represents a record for 0.74 eV p/n InGaAs. Calculations indicate that reducing the grid shadowing from the 16% on the test device to the 5% normally used in AM0 devices would increase the efficiency to >13%, a record for any 0.74 eV InGaAs (p/n or n/p).

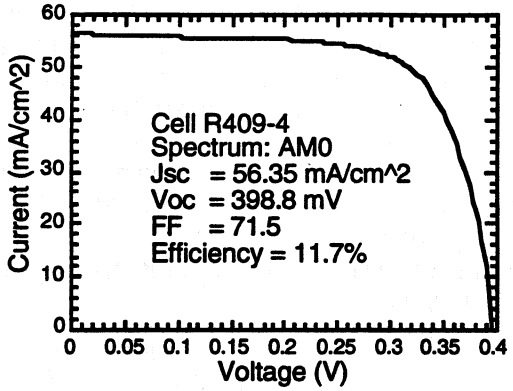

Figure 4.—I-V curve for baseline p/n cell

The external quantum efficiency for a 0.74 eV baseline device with a dual layer anti-reflective coating is shown in Figure 5. As was stated earlier, the base region was intentionally grown thin so that the effect of the BSR would be demonstrated. It was initially puzzling to observe the high bandedge photoresponse from the conventional cell (with no BSR). Optical modeling indicates that only 62% of the bandedge photons (1600 nm) are absorbed in the thin base region, assuming a single pass. Thus, the internal QE could not be greater than 62%. At 1600 nm the baseline device demonstrated a 74% internal QE (66% external QE, 10% reflection). The transmission characteristic of a n^+ InP substrate was measured at 1600nm and indicated >45% transmission (not corrected for absorption and reflection). Thus, bandedge photons are able to reach the back contact, which is a very reflective, non-alloyed Au based contact. It is believed that this contact acts as a BSR, reflecting the bandedge photons back toward the active cell region. Our past p/n devices had all utilized a sintered contact, which forms a highly absorbing Au_2P_3 compound at the semiconductor/metal interface. The QE characteristics of these devices did not demonstrate this enhanced bandedge photoresponse.

A negative aspect of this feature is that the reflection is diffuse in nature. Thus non-convertible photons may be totally internally reflected and add to the thermal load of the cell. A benefit of the diffuse reflection is that convertible photons will generally have a longer path length in the active cell layers, improving the probability for absorption. Given the high absorption coefficient for InGaAs, this is a marginal benefit.

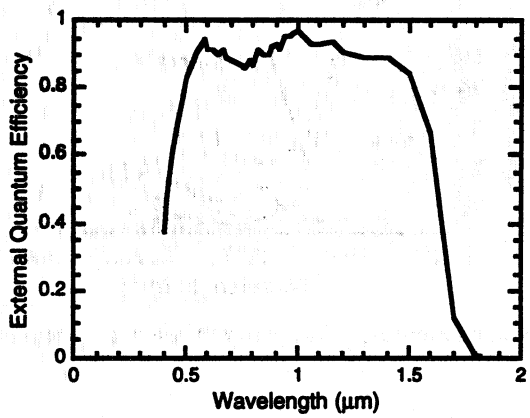

Figure 5.—External quantum efficiency for the 0.74 eV baseline InGaAs device.

The I-V curve for a 0.74eV MIM device is shown in Figure 6 under flashlamp testing. The data indicates an average voltage of 400 mV per cell. This particular device was produced prior to the development of the high quality Si_3N_4 dielectric and, therefore, is not expected to demonstrate optimum performance. The external QE curve for the 0.74eV device is shown in Figure 7 (without an anti-reflective coating). The QE data represents the aggregate worst

response from across the entire device, given the series interconnected nature of the MIM design. This device is expected to produce 48.5 mA when illuminated by a 1200 K blackbody emitter with a view factor of 1.

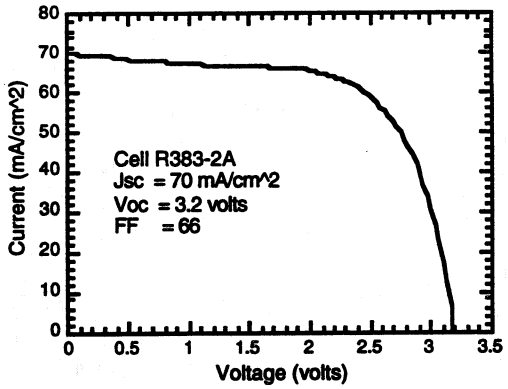

Figure 6.—I-V characteristic of 0.74 eV MIM under flashlamp testing (10 °C).

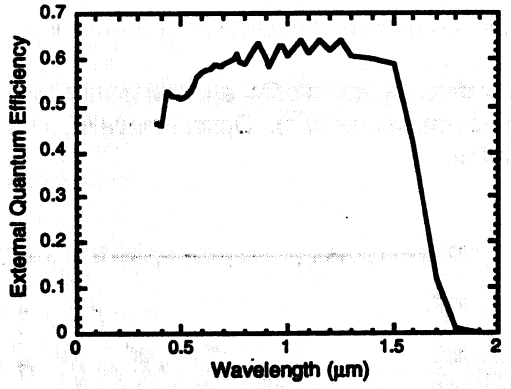

Figure 7.—External QE OF 0.74 eV MIM device without anti-reflective coating.

A 0.55 eV MIM was produced to determine if there were any unforeseen difficulties or problems in producing a MIM from lattice mismatched material. Figure 8 shows the I-V characteristic of a 0.55 eV MIM under AM0 testing. As with the 0.74 eV device reported above, this cell was produced prior to the optimization of the dielectric material. Unfortunately, this device was destroyed prior to I-V testing at higher injection levels.

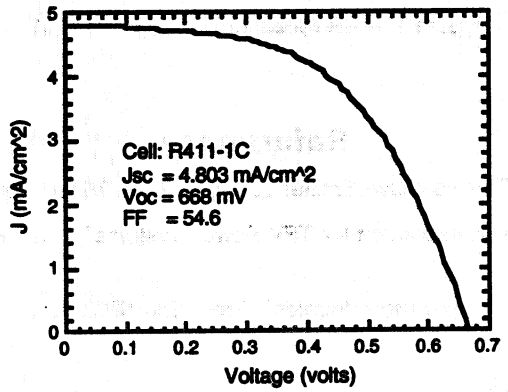

Figure 8.—AM0 I-V characteristic of 0.55 eV MIM (no AR).

Figure 9 shows the external QE characteristic for the 0.55 eV MIM (without AR). Given the rudimentary nature of the buffer layer used to produce this device and the limited development of the cell layers, the results were very promising.

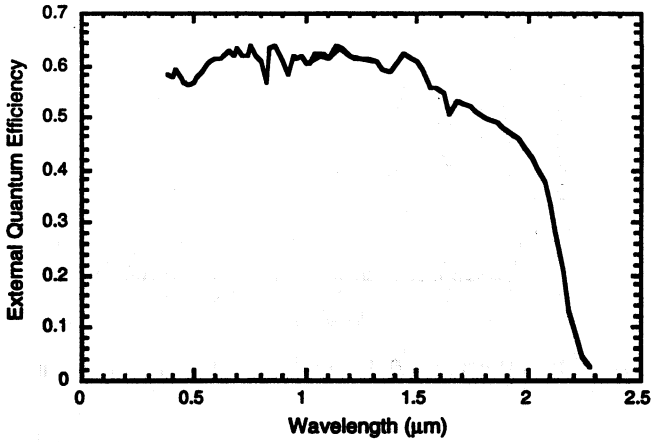

Figure 9.—External QE of 0.55 eV p/n MIM without AR.

Figure 10 shows the measured reflectivity for a 0.74 eV MIM device (without an AR coating). This particular device had a 3 μm LCL and a low doped emitter (1×10^{18}). Optical modeling suggests that IR reflectivity's of >90% are possible with optimized device structures.

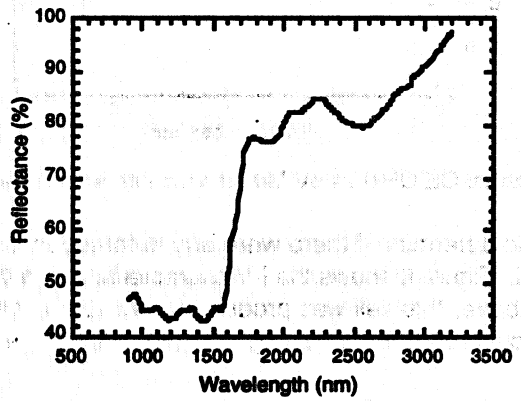

Figure 10.—IR reflectance of 0.74 eV MIM.

References

1. Chubb, D.L. and Lowe, R.L., "Thin-Film Selective Emitter", J. Appl. Phys. 79 (9), 1993, pp. 5687–5698.
2. Wilt, D.M., et al., "InGaAs PV Device Development for TPV Power Systems", 1st NREL Conf. on TPV Gen. of Elect., 1994, AIP 321, pp. 210.
3. Horne, W.E., et.al., "IR Filters for TPV Convertor Modules", Proc. 2nd NREL Conf. on TPV Gen. of Elect., 1995, AIP 358, pp. 35.
4. Woolf, L.D., Solar Cells **19**, 19 (1986).

5. Chubb, D.L., et.al., "Review of Recent TPV Research at Lewis Research Center", Proc. 14th SPRAT Conf, 1995, NASA CP–3324, pp. 191.

6. Charache, G.W., et.al., "Thermophotovoltaic Devices Utilizing a Back Surface Reflector for Spectral Control", Proc. 2nd NREL Conf. on TPV Gen. of Elect., 1995, AIP 358, pp. 339.

7. Iles, P.A. and Chu, C.L., "TPV Cells with High BSR", Proc. 2nd NREL Conf. on TPV Gen. of Elect., 1995, AIP 358, pp. 361.

8. Wojtczuk, S., "Multijunction InGaAs Thermophotovoltaic Power Convertor", Proc. 14th SPRAT Conf, 1995, NASA CP–3324, pp. 223.

9. Spitzer, M.B., et.al., "Monolithic Series-Connected Gallium Arsenide Convertor Development", Proc. IEEE 22nd PVSC, (1991), pp. 142–146.

10. Wilt, D.M., et al., "Monolithically Interconnected InGaAs TPV Module Development", Proc. IEEE 25th PVSC, (1996), pp. 43–48.

11. Wilt, D.M., et.al., "High Efficiency InGaAs Photovoltaic Devices for TPV Power Systems", Appl. Phys. Lett. 64 (18), 1994.